First Encapsulation of Organometallic Single-Molecule Magnet into Single-Walled Carbon Nanotubes

Haitao Zhang,[a],[b],[g]* Ryo Nakanishi,[b] Takefumi Yoshida,[c] Masahiko Nishijima,[d] Koji Harano,[e],[f] Yoji Horii,[h]* Masahiro Yamashita[a],[b]*

[a] Dr. H. Zhang, Dr. M. Yamashita
School of Chemical Science and Engineering
Tongji University
Siping Road 1239, Shanghai 200092, China
E-mail: zub.j.sad@gmail.com, Masahiro.yamashita.c5@tohoku.ac.jp

[b] Dr. H. Zhang, Dr. R. Nakanishi, Dr. M. Yamashita
Department of Chemistry, Graduate School of Science
Tohoku University
Sendai 980-8578, Japan

[c] Dr. T. Yoshida
Cluster of Nanomaterials, Graduate School of Systems Engineering
Wakayama University
930, Sakaedani, Wakayama 640-8510, Japan.

[d] Dr. M. Nishijima
Flexible 3D system Integration Laboratory, SANKEN
Osaka University
Mihogaoka 8-1, Ibaraki, Osaka 567-0047. Japan

[e] Dr. K. Harano
Department of Chemistry
The University of Tokyo
7-3-1 Hongo, Bunkyo-ku, Tokyo 113-0033, Japan

[f] Dr. K. Harano
Center for Basic Research on Materials
National Institute for Materials Science
1-1 Namiki, Tsukuba, Ibaraki 305-0044, Japan

[g] Dr. H. Zhang
Department of Chemistry
University of Hamburg
Harbor Bldg. 610 Luruper Chaussee 149, 22761 Hamburg, Germany

[h] Dr. Y. Horii
Department of Chemistry, Graduate School of Science
Nara Women's University
Kitauoya Higashimachi, Nara 630-8506, Japan
E-mail:horiiy20@cc.nara-wu.ac.jp

Supporting information for this article is given via a link at the end of the document.

Abstract: An air-sensitive $DyCp_3$ (Cp^-= cyclopentadienyl) single-molecule magnet (SMM) complex (**1**) was encapsulated into single-walled carbon nanotubes (SWCNTs) to construct hybrid materials that are resistant to moisture and oxygen. The hybrid materials with independent slow-magnetic-relaxing centers are expected to become a key component of the next generation of information process devices based on spintronics. The resilience to moisture and oxygen further broadens its manufacturing methods and application scenarios. Furthermore, upon encapsulation into SWCNTs, $DyCp_3$ exhibited clear ac frequency dependence in the ac magnetic susceptibility at a zero-dc field. This indicates that the guest molecule's slow magnetic relaxation properties are preserved, which is crucial and necessary to realize SMMs-based quantum information processing, by allowing a sufficient time window for quantum gate operations. Our result exemplifies that encapsulation of air-sensitive organometallic SMMs into SWCNTs enhances their chemical stability and their magnetic relaxation time at a zero-dc magnetic field, which provides a novel method for their further applications.

Single-molecule magnets (SMMs) have attracted great attention since the discovery of Mn_{12} cluster exhibiting magnetic bistability at the molecular level.[1] This unique magnetism makes the SMMs versatile candidates for use in spintronics devices such as ultrahigh density memory devices and quantum bit for quantum computers. The high operating temperature of the SMMs is one of the most critical performance indicators. From 2017 to the present, it has been reported that dysprosium complexes act as SMMs exhibiting high operating temperatures reaching as high as 60 – 80 K.[2] Such organometallic complexes based on cyclopentadienyl (Cp^-) ligands have great advantages for high-performance SMMs due to large ligand field splitting induced by the convergent negative charge of Cp^-, and fewer phonon modes causing the Raman process.[3] However, the lanthanoid Cp^- complexes are highly moisture sensitive, making them difficult to

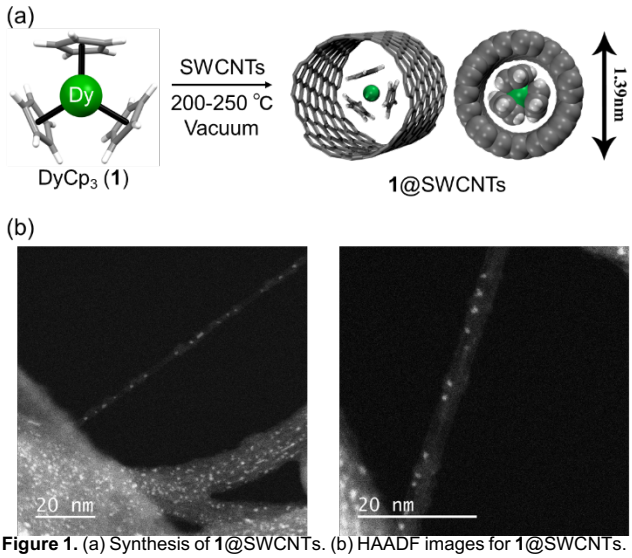

Figure 1. (a) Synthesis of **1**@SWCNTs. (b) HAADF images for **1**@SWCNTs. The bright spots attributed to the **1**.

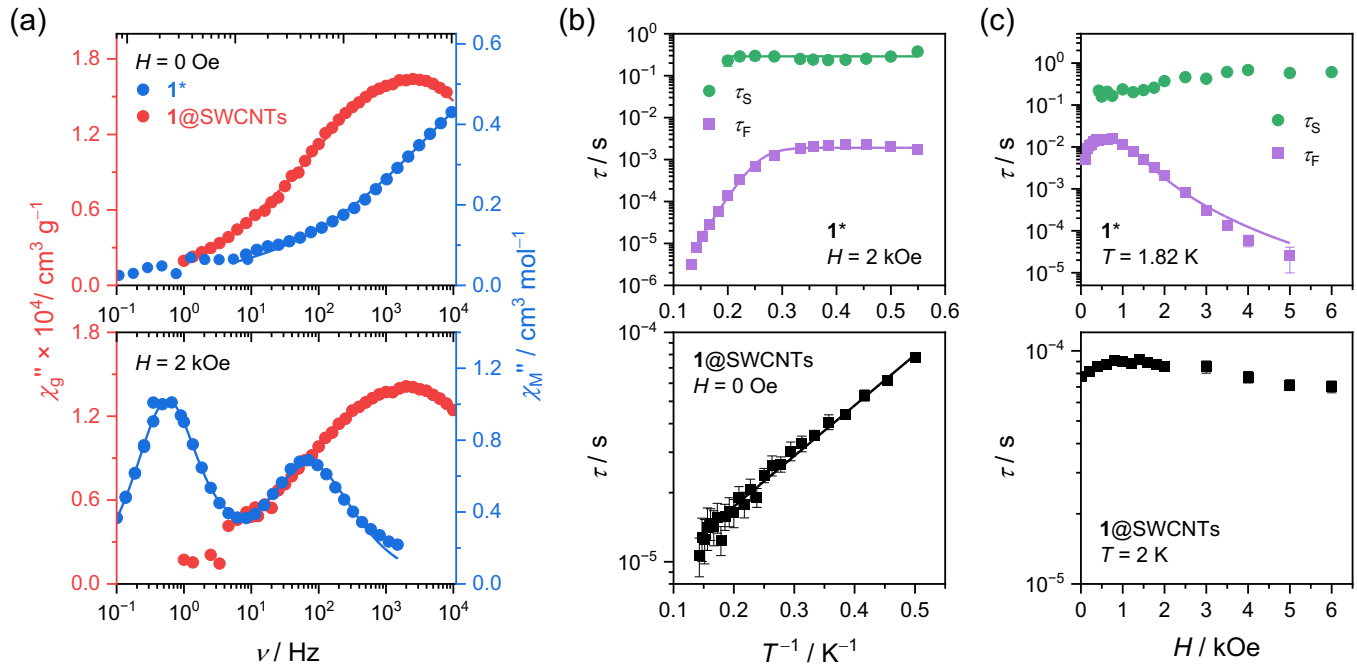

Figure 2. (a) Imaginary part of the ac magnetic susceptibility at 2 K at a dc magnetic field of 0 Oe (upper) and 2 kOe (lower) for **1*** and **1**@SWCNTs. The data for **1*** at H = 0 Oe in the ν range < 130 Hz was acquired at 1.82 K. The data in the ν range < 10 Hz were acquired using MPMS and scaled by 0.98 at 0 Oe and by 0.95 at 2 kOe. The unit of the magnetic susceptibilities for **1*** and **1**@SWCNTs are per mole (χ_M'') and per gram (χ_g''), respectively. (b) Arrhenius plots for **1*** (upper) and **1**@SWCNTs (lower). (c) H dependence of the τ values for **1*** (upper) and **1**@SWCNTs (lower).

construct spintronic devices in a pristine form. Apart from the Cp^--based SMMs, the fullerene-based SMMs with lanthanide clusters protected by the fullerene cage have been reported as examples combining high operating temperature and chemical stability.[4] In a similar manner to the fullerene cages, single-walled carbon nanotubes (SWCNTs) are also effective in protecting chemically unstable substances, including organometallic SMMs, from the air and moisture, facilitating the handling of the SMM-SWCNTs hybrid materials. The encapsulation of the dysprosium SMMs into the SWCNTs has been investigated theoretically by Nabi *et al.* based on the CASSCF and DFT calculations.[5] It is noteworthy that the ligand field splitting of Dy^{3+} ions depends on the orientation of the dysprosium-SMM molecule in the SWCNT, and in some cases, the activation energy for spin reversal is enhanced upon encapsulation. These results suggest that the encapsulation of air-sensitive SMMs is valid for protecting and improving SMM properties. Regarding device fabrication, the SMM-SWCNTs hybrid materials constructed by anchoring the SMMs to the surface of SWCNTs[6] have been used for the component of molecular spin valves exhibiting spin-dependent electrical current.[7] In this method, the spin information stored in the SMM can be read out using the change in current. In addition to the anchoring approach, the construction of hybrid materials based on encapsulation has been reported for various kinds of SMMs.[8] It should be noted that the SMMs used in the encapsulation (Mn_{12},[1] $DySc_2N@C_{80}$,[4b] $Dy_2ScN@C_{80}$,[4c] $TbPc_2$,[9] $Dy(acac)_3{\cdot}2H_2O$[10]) are charge neutral, and have highly symmetrical structures except for $Dy(acac)_3{\cdot}2H_2O$. The latter factor minimizes a permanent electric dipole moment, indicating that a molecule with a negligible electric dipole moment is preferable for encapsulation. This idea is supported by the fact that molecules with low polarity such as C_{60},[11] coronene[12] ,and P_4[13] have been smoothly encapsulated into the nanotubes.

In this work, we report the encapsulation of tris(cyclopentadienide)dysprosium $DyCp_3$ (**1**) into SWCNTs using a sublimation method. **1** has an equilateral triangle structure in which vertices coincide with the centroid of Cp^- rings, and the Dy^{3+} ion is located at the centroid of **1** (Figure 1). Such a highly symmetrical structure suppresses the inter–$DyCp_3$–molecular interactions originating from the permanent electric dipole moment. Due to its charge-neutral nature, **1** can be sublimated at a relatively mild temperature (220-250 °C) under vacuum[14], enabling the encapsulation into SWCNTs using the sublimation method, which provides less contamination compared to the capillary method using solvents. On the other hand, **1** is highly sensitive to moisture, making its handling in the air difficult. Therefore, the encapsulation of **1** to the SWCNTs improves its usability which is essential for manufacturing. Before the encapsulation, the SWCNTs were cleaned using dispersion, acid treatment, and sublimation to remove the paramagnetic metal catalysts (see SI). **1** with a molecular size of *ca.* 0.7 nm was encapsulated into the SWCNTs with a diameter of 1.4 ± 0.1 nm using a sublimation method at 200-250 °C under high vacuum to form hybrid material **1**@SWCNTs. The diluted **1** sample did not show clear slow magnetic relaxations at a zero-dc-bias field, whereas **1**@SWCNTs exhibited clear slow magnetic relaxation behaviors at a zero-dc-bias field. These results indicated the enhanced SMM properties upon encapsulation.

To check the encapsulation of **1** into SWCNTs, scanning transmission electron microscope (STEM) measurements were performed for **1**@SWCNTs. Heavy atoms (*i.e.*, Dy) can scatter electrons to higher angles. Therefore, they show strong contrast under a high-angle annular dark-field (HAADF) mode. Thus, **1** appears as a bright spot in the HAADF images (Figure 1(b)). Meanwhile, the outlines of SWCNTs can be clearly identified in

the bright field (BF) images. (Figure S5). Electron energy-loss (EELS) spectroscopy for the selected bright spots exhibits the characteristic peak of the Dy element (Figure S6). As shown in the enlarged view of **1**@SWCNTs, the bright spots were sparsely distributed, indicating **1** does not tend to form continuous nanocrystals within SWCNTs. In addition, no bulk crystalline **1** was found depositing on the out-surface of SWCNTs. A bundle of **1**@SWCNTs illuminated at a lower magnification under a TEM mode corroborates that the encapsulation is not just a result within a specific region. The corresponding energy-dispersive X-ray (EDX) spectroscopy (Figure S7) shows the characteristic peaks of the Dy element. Real-time high-resolution TEM images and videos and more relevant discussion can be found within the supplementary materials

To get the information about the coordination structure around the Dy atom, X-ray absorption fine structure (XAFS) was acquired for **1** and **1**@SWCNTs. The white line peak intensity in the XANES spectra for **1**@SWCNTs is slightly larger than that of **1**, indicating that some of the Dy species in **1**@SWCNTs is slightly oxidized (Figure S8). Based on the Dy L_3-edge EXAFS for **1** and **1**@SWCNTs, the bond distances of Dy-C and coordination numbers derived as 2.38 Å and 13.8 ± 1.2 for **1** and 2.40 Å and 16.8 ± 3.1 for **1**@SWCNTs (Figures S9, S10 and Table S1, S2), respectively, indicating that the coordination structure of **1** is maintained in **1**@SWCNTs. The amount of the **1** in **1**@SWCNTs was further checked by X-ray photoelectron spectroscopy (XPS), as shown in Figure S11. The double peaks of the Dy element were observed in **1**@SWCNTs. The carbon peak of **1**@SWCNTs was broadened compared to that of pure SWCNTs, presumably due to interactions between **1** and SWCNTs. All peaks were fitted by the Voigt GL(30) function while fixing the ratio of peak area accounting for the spin-orbit coupling degeneracy. The encapsulation ratio of **1** based on the relative peak intensity corrected by relative sensitivity factors was 10.5%, which is close to the value estimated from magnetic data, as discussed later (Figure S16). To check the changes in the electronic structure of the SWCNTs upon encapsulation, Raman spectra were acquired for pure SWCNTs and **1**@SWCNTs. The G band for the SWCNTs that corresponds to the sp^2 hybridized carbon system[15] shifted to the lower frequency region due to interactions between SWCNTs and **1** (Figure S4). The intermolecular interactions change the charge distribution on the surface of SWCNT and the Cp^- ligands (Figure S25).

To check the SMM properties, dc magnetic measurements were performed for a magnetically diluted sample of **1**, hereafter identified as **1***. Nakanishi *et al*. have reported that the encapsulation of the SMMs into SWCNTs acts as if SMMs are magnetically diluted because the filling ratio of the SMMs is around 10 wt%.[8d, 8f] Therefore, the comparison of the magnetism of **1*** and **1**@SWCNTs can extract the effect of encapsulation on the SMM properties. The successful synthesis of $Dy_{0.075}Y_{0.925}Cp_3$ (**1***) was confirmed by the powder X-ray diffraction analyses, which show an excellent agreement with the simulated pattern for the reported single-crystal X-ray structural data for YCp_3 (Figure. S2).[16] $\chi_M T$ vs. T plots of **1*** at a dc magnetic field of 1 kOe are shown in Figure S12. The $\chi_M T$ value at 300 K is 14.15 cm^3 K mol^{-1}, which is close to the theoretical value (14.17 cm^3 K mol^{-1}). The gradual decrease in the $\chi_M T$ value upon decreasing T is attributed to the thermal depopulation of the Stark sublevels rather than the intermolecular magnetic interactions, the latter of which are negligible in **1*** due to magnetic dilution. Magnetization as a function of the magnetic field at 1.82 K did not show hysteresis behavior due to fast magnetic relaxation (Figure S13).

DC magnetic susceptibility of **1**@SWCNT at a dc field of 1 kOe shows a decrease in $\chi_g T$ with decreasing T (Figure S14). The linear decrease in the high T region corresponds to the small amount of magnetic impurities attributable to metal catalysts. The contribution of the magnetic impurities is less dominant at the low T region due to the paramagnetism of **1** in SWCNTs. The decrease in the $\chi_g T$ value at the low T region corresponds to the thermal depopulation of the Stark sublevels, as observed in **1***. M vs. H curves did not show magnetic hysteresis behavior at 1.82 K due to fast magnetic relaxations (Figure S15). The encapsulation ratio of the $DyCp_3$ in the SWCNTs estimated from the comparison of magnetization curves for **1**@SWCNT and **1*** is *ca.* 9.9 wt% (Figure S16), which is close to the value estimated from XPS measurements, and the value reported for fullerene-based SMMs encapsulated into the SWCNTs.[8d, 8f]

Figure 2(a) summarizes the selected ac magnetic susceptibility data for **1*** and **1**@SWCNTs at 2 K. In the case of **1***, ac frequency (v) dependence was observed at a zero-dc magnetic field, confirming that **1** is an SMM. However, the peak top of χ_M'' could not be observed in the measured v range. In the case of **1**@SWCNTs, the broad but clear peak top was observed even at zero-dc magnetic field, indicating that zero-field magnetic relaxations are suppressed upon encapsulation. This is a rare example of encapsulation enhancing the SMM properties.[8d] In the case of **1***, clear χ_M'' peaks were observed at the non-zero-dc field, which is attributed to the quenching of quantum tunneling of the magnetization (QTM) by the Zeeman effect. As shown in Figure 2(a), two peaks were observed in the imaginary part of the ac magnetic susceptibilities at a dc field of 2 kOe. The dual magnetic relaxations for **1*** are possibly attributed to the two kinds of crystallographically inequivalent **1** unit in the crystal packing.[17]

To extract the magnetic relaxation times τ from the ac magnetic susceptibilities, fitting based on the generalized Debye model[18] was performed for **1***. T-dependence of the slower (τ_S) and faster (τ_F) relaxation times at a dc field of 2 kOe is summarized in Figure 2(b). The τ_S is T independent in the measured T range, whereas τ_F at high T region was T dependent. The τ_F was simulated with the following equation:

$$\tau^{-1} = {\tau_{QTM}}^{-1} + {\tau_0}^{-1}\exp\left(-U_{eff}/k_B T\right) \qquad \text{Eq. 1}$$

where first and second term represents QTM and Orbach process, respectively, with the optimized parameters ${\tau_{QTM}}^{-1}$ = 5.2(3) × 10^2 s^{-1}, ${\tau_0}^{-1}$ = 7(2) × 10^7 s^{-1} and U_{eff} = 32(1) cm^{-1}. In the case of τ_{SR}, ${\tau_{QTM}}^{-1}$ = 3.5(2) s^{-1} was obtained from the fitting based on Eq. 1.

To validate the SMM properties of **1***, complete active space self-consistent field (CASSCF) method and spin-orbit (SO) coupling calculations were performed for two kinds of **1** unit, namely **1**A and **1**B (see SI). The structures of **1**A and **1**B are similar, but a significant difference in the magnetism was found based on the *ab initio* calculation. The ground ligand field sublevels of **1**A are composed of 80% of M_J = ±15/2, whereas those of **1**B are composed of 46.9% of M_J = ±15/2 and 21.9% of M_J = ±11/2,

indicating that the ground doublet of **1**B is less axially anisotropic (Tables S14 and S15). The energy difference between ground and first excited Kramers levels are 69 cm^{-1} for **1**A and 45 cm^{-1} for **1**B (Table S13), which are similar in magnitude to the experimental U_{eff} value, indicating the Orbach process via first excited Kramers doublet.

In contrast with **1***, ac magnetic susceptibility of **1**@SWCNTs at zero-dc magnetic field exhibited a broad χ_g'' peak that can be simulated using the generalized Debye model (Figure 2(a)). To check the *T*-dependence of the τ values, ac magnetic measurements were performed at zero-dc magnetic field in the *T* range 2-7 K (Figure S18). The τ values in the *T* range 2-7 K obeys Arrhenius behavior with the U_{eff} of 3.53(7) cm^{-1} and τ_0^{-1} = 1.6(6) × 10^5 s^{-1} (Figure 2(b)). The U_{eff} value of **1**@SWCNT is small compared with **1*** and other reported SMMs.[4b, 8d, 8f] One possible explanation is the under-barrier relaxations via anharmonic phonon.[19]

The magnetic field dependence of the τ values was also checked for **1*** and **1**@SWCNTs (Figures S17 and S19). In the case of **1***, the single χ_M'' peak attributable to τ_F was observed in the *H* range of 100-370 Oe. Above 430 Oe, the small shoulder appears at the lower *v* region. This lower shoulder became dominant with increasing *H*, while the peak at the high *v* region diminished. The *H* dependence of the τ_S and τ_F are summarized in Figure 2(c). τ_S exhibited a tiny increase with increasing *H* range, whereas τ_F increases with increasing the *H* up to 750 Oe, and decreases above 1 kOe. τ_F was reasonably simulated by the following equation:

$$\tau^{-1} = aH^4 + B(1 + CH^2)/(1 + DH^2) \qquad \text{Eq. 2}$$

where the first and second terms represent direct process and QTM with the optimized parameters, *a* = 3.2(1) × 10^{-11} s^{-1} Oe^{-4}, *B* = 1.5(5) × 10^{-2} s^{-1}, *C* = 1.1(7) × 10^{-5} s^{-1} Oe^{-2} and *D* = 3(3) × 10^{-5} s^{-1} Oe^{-2}. Similar behaviors have been observed in other Dy-based SMMs. In the weak dc field, the suppression of QTM increases τ value. Further increase in the *H* induces a direct process, thereby decreasing the τ value. As a result, τ_F vs. *H* plots show a peak at the optimized dc magnetic field.

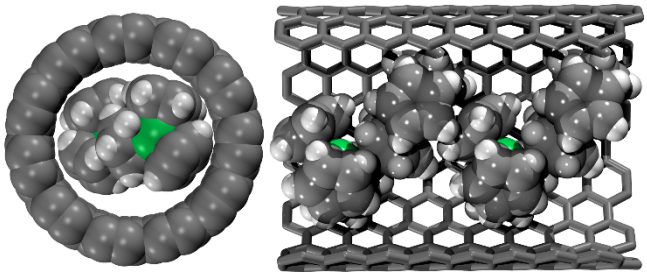

Figure 3. The optimized structure **1**$_2$@n11m11-type3.

The magnitude of τ values for **1**@SWCNTs is similar to that of τ_F in **1***, and *H* dependence of τ shows very broad peak at around 1 kOe (Figure 2(c)). However, the fitting based on Eq. 1 is unsuccessful due to very weak *H* dependence of τ values.

Although STEM measurements support the encapsulation of **1** in the SWCNTs, the packing structure of **1** inside the SWCNTs could not be directly determined, due to its low real-space resolution. It is also not simple to make a single **1** molecular observation using a TEM mode, as electron beam-induced polymerization occurs even in a very short time scale (see SI). In order to obtain the geometric structure of the encapsulated **1** inside the SWCNTs, the geometric structure optimizations and single-point energy evaluations with periodic boundary conditions (PBC) were performed using the PBE exchange–correlation functional with the Grimme's DFT-D3 dispersion correction.[20] Three kinds of SWCNTs with diameters of around 1.4 nm were selected as the supercell structural units (around 10 Å), and 16 kinds of encapsulation scenarios were considered for binding energy (E_B) calculations (Table S11). Among them, the two **1** units encapsulated in the SWCNT (n11m11) fragment while keeping the C_3 axis of the adjacent molecules nearly perpendicular to each other (**1**$_2$@n11m11-type3 shown in Figure 3), exhibited the lowest E_B (−139.86 kJ mol^{-1}). This E_B is lower than the **1**A and **1**B in the crystal packing (Table 1), suggesting the spontaneous encapsulation of **1** into SWCNTs. The upper limit of the mass ratio of **1**$_2$@11n11m-type3 (25.29%) is larger than the experimental values, indicating that such packing structures are sparsely present in the **1**@SWCNTs. Real-time TEM for **1**@SWCNTs (Figure S26) afforded the shadow of the row of circles resembling to the simulated TEM image of **1**$_2$@11n11m-type3.

CASSCF calculations using the geometries of **1**$_2$@11n11m-type3 revealed an axial magnetic anisotropy with the g_z values of 14.97 and 15.62, which is slightly larger than that of **1**B (g_z = 14.81) but lower than that of **1**A (g_z = 17.94) in the crystal packing. On the other hand, CASSCF calculations using **1**@n18m0-type1 with smaller E_B (−114.12 kJ mol^{-1}) and optimized geometry of **1** in the vacuum predicted an in-plane magnetic anisotropy (Table 1). Our results suggest that the magnetism of **1** is sensitive to the subtle conformation changes upon encapsulation. This explains why the broad χ_g'' peak was observed in **1**@SWCNTs. The conformational variations upon encapsulations increase the dispersion of τ value, resulting in the broad χ_g'' peak.

Table 1. Principal *g* values of the ground Kramers doublet and binding energies (E_B) of the selected systems based on PBE-D3 KS-DFT.

	g_x	g_y	g_z	E_B / kJ mol^{-1}
1A[a]	0.489	1.850	17.938	−122.06[b]
1B[a]	0.994	5.764	14.810	
1$_2$@11n11m type3	0.985	5.626	14.967	−139.86
	0.917	4.867	15.616	
1@18n0m type1	11.045	10.013	1.196	−114.12
1 (vacuum)	10.548	10.514	1.196	-

[a] Based on the crystal coordinates of YCp_3 in ref .[16b] [b] Based on the DFT optimized packing structure.

In conclusion, we have successfully synthesized the hybrid material composed of organometallic SMM and SWCNTs utilizing the vacuum sublimation method. The hybrid material is stable in

the air and easy to handle even though the pristine SMM used in this research is highly sensitive to the air. This work also validates that SWCNTs, as showcases, can preserve the delicate power of organometallic SMMs, expanding the latter's potential applications. Importantly, the encapsulation of **1** suppresses the magnetic relaxations at a zero-dc bias field, enhancing the SMM properties.

Acknowledgements

This work was supported by JSPS KAKENHI Grant Number JP19H05631 (M. Y.), the National Natural Science Foundation of China (NSFC, 22150710513). M. Y. acknowledges the support by the 111 project (B18030) from China. K. H. acknowledges the support by JSPS KAKENHI Grant Number JP23H04874. H. Z. acknowledges the financial support by the German Research Foundation (DFG) *via* projects HE-5675/6-1 and GRK 2536 NANOHYBRID. R. N and H. Z. thank Dr. Takamichi Miyazaki for his assistance during TEM measurements. H. Z. thanks Prof. Dr. Carmen Herrmann for the valuable dissociations and support. H. Z. thanks the High-Performance Computing Center at University of Hamburg and the North-German Supercomputing Alliance (HLRN) for computational resources. XAFS was collected on the BL-12C beamline in the Photon Factory of the High Energy Accelerator Research Organization (KEK, proposal no. 2017P013).

Keywords: single-molecule magnet • carbon nanotube • hybrid material

[1] R. Sessoli, D. Gatteschi, A. Caneschi, M. Novak, *Nature* **1993**, *365*, 141-143.

[2] (a)C. A. P. Goodwin, F. Ortu, D. Reta, N. F. Chilton, D. P. Mills, *Nature* **2017**, *548*, 439-442; (b)F.-S. Guo, B. M. Day, Y.-C. Chen, M.-L. Tong, A. Mansikkamäki, R. A. Layfield, *Angew. Chem. Int. Ed.* **2017**, *56*, 11445-11449; (c)F.-S. Guo, B. M. Day, Y.-C. Chen, M.-L. Tong, A. Mansikkamäki, R. A. Layfield, *Science* **2018**, *362*, 1400-1403; (d)C. A. Gould, K. R. McClain, D. Reta, J. G. C. Kragskow, D. A. Marchiori, E. Lachman, E.-S. Choi, J. G. Analytis, R. D. Britt, N. F. Chilton, B. G. Harvey, J. R. Long, *Science* **2022**, *375*, 198-202.

[3] A. Chiesa, F. Cugini, R. Hussain, E. Macaluso, G. Allodi, E. Garlatti, M. Giansiracusa, C. A. P. Goodwin, F. Ortu, D. Reta, J. M. Skelton, T. Guidi, P. Santini, M. Solzi, R. De Renzi, D. P. Mills, N. F. Chilton, S. Carretta, *Physical Review B* **2020**, *101*, 174402.

[4] (a)Z. Hu, Y. Wang, A. Ullah, G. M. Gutiérrez-Finol, A. Bedoya-Pinto, P. Gargiani, D. Shi, S. Yang, Z. Shi, A. Gaita-Ariño, E. Coronado, *Chem. Eur. J.* **2023**; (b)R. Westerström, J. Dreiser, C. Piamonteze, M. Muntwiler, S. Weyeneth, H. Brune, S. Rusponi, F. Nolting, A. Popov, S. Yang, L. Dunsch, T. Greber, *J. Am. Chem. Soc.* **2012**, *134*, 9840-9843; (c)R. Westerström, J. Dreiser, C. Piamonteze, M. Muntwiler, S. Weyeneth, K. Krämer, S.-X. Liu, S. Decurtins, A. Popov, S. Yang, L. Dunsch, T. Greber, *Physical Review B* **2014**, *89*, 060406; (d)F. Liu, D. S. Krylov, L. Spree, S. M. Avdoshenko, N. A. Samoylova, M. Rosenkranz, A. Kostanyan, T. Greber, A. U. B. Wolter, B. Büchner, A. A. Popov, *Nat. Commun.* **2017**, *8*, 16098.

[5] R. Nabi, R. K. Tiwari, G. Rajaraman, *Chem. Commun.* **2021**, *57*, 11350-11353.

[6] S. Kyatskaya, J. R. Galán Mascarós, L. Bogani, F. Hennrich, M. Kappes, W. Wernsdorfer, M. Ruben, *J. Am. Chem. Soc.* **2009**, *131*, 15143-15151.

[7] M. Urdampilleta, S. Klyatskaya, J. P. Cleuziou, M. Ruben, W. Wernsdorfer, *Nature Materials* **2011**, *10*, 502.

[8] (a)M. del Carmen Giménez-López, F. Moro, A. La Torre, C. J. Gómez-García, P. D. Brown, J. van Slageren, A. N. Khlobystov, *Nat. Commun.* **2011**, *2*, 407; (b)R. Nakanishi, M. A. Yatoo, K. Katoh, B. K. Breedlove, M. Yamashita, *Materials* **2017**, *10*, 7; (c)S. M. Avdoshenko, F. Fritz, C. Schlesier, A. Kostanyan, J. Dreiser, M. Luysberg, A. A. Popov, C. Meyer, R. Westerström, *Nanoscale* **2018**, *10*, 18153-18160; (d)R. Nakanishi, J. Satoh, K. Katoh, H. Zhang, B. K. Breedlove, M. Nishijima, Y. Nakanishi, H. Omachi, H. Shinohara, M. Yamashita, *J. Am. Chem. Soc.* **2018**, *140*, 10955-10959; (e)K. Katoh, J. Sato, R. Nakanishi, F. Ara, T. Komeda, Y. Kuwahara, T. Saito, B. K. Breedlove, M. Yamashita, *J. Mater. Chem. C* **2021**, *9*, 10697-10704; (f)S. Ito, R. Nakanishi, K. Katoh, B. K. Breedlove, T. Sato, Z.-Y. Li, Y. Horii, M. Wakizaka, M. Yamashita, *Dalton Trans.* **2022**, *51*, 6339-6344.

[9] (a)N. Ishikawa, M. Sugita, T. Ishikawa, S.-y. Koshihara, Y. Kaizu, *J. Am. Chem. Soc.* **2003**, *125*, 8694-8695; (b)N. Ishikawa, M. Sugita, N. Tanaka, T. Ishikawa, S.-y. Koshihara, Y. Kaizu, *Inorg. Chem.* **2004**, *43*, 5498-5500.

[10] S. D. Jiang, B. W. Wang, G. Su, Z. M. Wang, S. Gao, *Angew Chem Int Ed Engl* **2010**, *49*, 7448-7451.

[11] B. W. Smith, M. Monthioux, D. E. Luzzi, *Nature* **1998**, *396*, 323-324.

[12] T. Okazaki, Y. Iizumi, S. Okubo, H. Kataura, Z. Liu, K. Suenaga, Y. Tahara, M. Yudasaka, S. Okada, S. Iijima, *Angew. Chem. Int. Ed.* **2011**, *50*, 4853-4857.

[13] M. Hart, E. R. White, J. Chen, C. M. McGilvery, C. J. Pickard, A. Michaelides, A. Sella, M. S. P. Shaffer, C. G. Salzmann, *Angew. Chem. Int. Ed.* **2017**, *56*, 8144-8148.

[14] J. M. Birmingham, G. Wilkinson, *J. Am. Chem. Soc.* **1956**, *78*, 42-44.

[15] M. S. Dresselhaus, G. Dresselhaus, R. Saito, A. Jorio, *Physics Reports* **2005**, *409*, 47-99.

[16] (a)M. Adam, U. Behrens, R. D. Fischer, *Acta Crystallogr. C* **1991**, *47*, 968-971; (b)S. M. J. Beer, A. Krusenbaum, M. Winter, C. Vahlas, A. Devi, *Eur. J. Inorg. Chem.* **2020**, *2020*, 3587-3596.

[17] U. Baisch, S. Pagano, M. Zeuner, J. Schmedt auf der Günne, O. Oeckler, W. Schnick, *Organometallics* **2006**, *25*, 3027-3033.

[18] N. Domingo, F. Luis, M. Nakano, M. Muntó, J. Gómez, J. Chaboy, N. Ventosa, J. Campo, J. Veciana, D. Ruiz-Molina, *Phys. Rev. B* **2009**, *79*, 214404.

[19] A. Lunghi, F. Totti, R. Sessoli, S. Sanvito, *Nat. Commun.* **2017**, *8*, 14620.

[20] S. Grimme, J. Antony, S. Ehrlich, H. Krieg, *J. Chem. Phys.* **2010**, *132*, 154104.

Entry for the Table of Contents

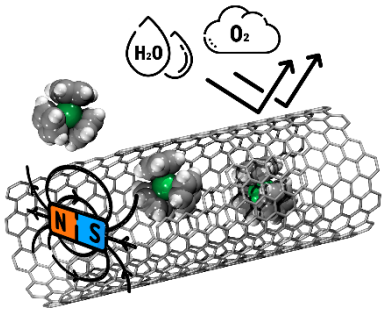

Encapsulating chemically unstable organometallic single-molecule magnets in single-walled carbon nanotubes not only improves their chemical stability but also suppresses magnetic relaxation at zero magnetic fields, greatly improving their usability, which is essential for fabricating spintronic devices.

Institute and/or researcher Twitter usernames: ((optional))